HEP'99 # 4_518
Submitted to Pa 4, 5
Pl 4, 5

DELPHI 99-107 CONF 294
15 June 1999

New precise measurement of V_{cb}

Preliminary

DELPHI Collaboration

Paper submitted to the HEP'99 Conference
Tampere, Finland, July 15-21

New precise measurement of V_{cb}

Preliminary

DELPHI Collaboration

M.Margoni,F.Simonetto
Comments to: franco.simonetto@padova.infn.it

New precise measurements of V_{cb} and of the branching ratios BR($\bar{B}^0 \to D^{*+}\ell\bar{\nu}$), BR($b \to D^{*+}\ell\bar{\nu}X$), are obtained. They are based on a sample of $\sim$ 7000 semileptonic decays $b \to D^{*+}\ell\bar{\nu}X$, selected out of $\sim$ 3 million hadronic Z decays collected by the DELPHI detector at LEP I, by tagging the soft pion from $D^{*+} \to D^0\pi^+$.
The analytic dependence of the differential cross section and of the form factor as a function of the variable $w = v_{B^0} \cdot v_{D^*}$ are also obtained by folding out the experimental resolution.

1 Introduction

In the framework of the Standard Model, the coupling among quarks of different flavours is described by the Cabibbo-Kobayashi-Maskawa (CKM) matrix. Its elements are not predicted by the theory, apart from the constraints due to the requirement of unitarity.

A precise measurement of $|V_{cb}|$, the element corresponding to the beauty to charm transitions, allows to constrain the parameters which describe the process of CP violation for $\bar{B}^0_d$ mesons[†] [1]. Progress in the phenomenological description of heavy flavour semileptonic decay allows to determine $|V_{cb}|$ with small theoretical systematic error, from either the inclusive process $b \to c\ell\bar{\nu}$, or from an analysis of the form factors in the decay $\bar{B}^0_d \to D^{*+}\ell^-\nu$. The present measurement is based on the second approach [2].

The decay rate for the last process is proportional to $|V_{cb}|^2$ and to the hadron matrix elements describing the transition from a $\bar{B}^0_d$ to a D^{*+} meson. In the limit of very heavy quarks ($m_{b,c} >> \Lambda_{QCD} \sim 200\ MeV/c^2$), the amplitude is proportional to a single form factor $\mathcal{F}(w)$, where w is the product of the $\bar{B}^0_d$ and D^{*+} four velocities. When $w = 1$ the D^{*+} is produced at rest in the $\bar{B}^0_d$ rest frame: as a consequence of Heavy Flavour symmetry, the normalisation $\mathcal{F}(1) = 1$ is expected. Corrections to this prediction due to perturbative QCD have been computed up to second order in [3]; the effect of finite b, c quarks masses has been calculated in the frame of Heavy Quark Effective Theory [4]. They finally yield $\mathcal{F}(1) = 0.91 \pm 0.03$ [5].

The measurement of the decay rate at $w = 1$ would therefore allow to determine $|V_{cb}|$ with small theoretical uncertainty. Due to phase space suppression, this quantity is determined from the extrapolation at 1 of the differential rate $\mathrm{d}\Gamma/\mathrm{d}w$, where $\mathcal{F}(w)$ is parametrised following several different functional forms [5, 6] (see also discussion below).

Results based on this approach were reported by the ARGUS [7] and CLEO [8] collaborations operating at the $\Upsilon(4S)$ and by ALEPH [9, 10] and OPAL [11] at LEP. The present paper updates the previous DELPHI result of [12]. Identification of D^{*+} mesons is based on the tagging of the soft pion (π^*) from the decay $D^{*+} \to D^0\pi^+$, the method referred to as "inclusive analysis" in [12]. As compared to this previous work, the following improvements were obtained:

- the resolution on w was improved by a factor ~ 1.5 by applying the algorithm of inclusive secondary vertex reconstruction developed for $\bar{B}^0_d$ lifetime [13] and oscillation [14] measurements;
- the full available statistics was analysed, so increasing the sample by more than a factor two;
- the most recent parametrisation [6] of $\mathcal{F}(w)$ was used to extrapolate the experimental data at w =1;
- the fraction of events in the sample due to intermediate production of higher excited charm states (decaying into $D^{*+}\,\pi$ or into $D^{*+}\,\pi\pi$, in the following collectively designated as D^{**}) was determined in this same data sample, with a method independent of the one used in [12]. As a consequence, a result for the product of branching ratios $\mathrm{BR}(b \to D^{**}l\bar{\nu}) \times \mathrm{BR}(D^{**} \to D^{*+}X)$ was obtained as well.

[†]Charge conjugated states are always implied; lepton (ℓ) means either an electron or a muon, unless the contrary is explicitly stated.

2 The DELPHI detector

The DELPHI detector has been described in detail elsewhere [15]. Charged particle tracking through the uniform axial field (B = 1.23 T), secondary vertex reconstruction and lepton identification are important in this analysis: they will be shortly described in the following.

The detector elements used for tracking are the Vertex Detector (VD), the Inner Detector (ID), the Time Projection Chamber (TPC), the Outer Detector (OD) and the Forward Chambers in the endcap regions. The average momentum resolution for high momentum (p) charged particles is $\sigma(p)/p = 0.0006\ p$ (GeV/c), in the polar region between 30^o and 150^o.

The VD, consisting of 3 cylindrical layers of silicon detectors (radii 6, 8 and 11 cm), provides up to 3 hits per track (or more in small overlapping regions) in the polar angle range $43^o < \theta < 137^o$. In the original design the VD only provided two dimensional information in the plane $R\phi$, orthogonal to the beam direction. Since the 1994 data taking, an upgraded detector with full three-dimensional point reconstruction was installed. In the $R\phi$ direction the spatial resolution of the VD is $\sim$ 8μm per point: tracks from charged particles are extrapolated back to the beam collision point with a resolution of $\sqrt{20^2 + 65^2/p_\perp^2}$, where $p_\perp$ is the momentum of the particle in the $R\phi$ plane. The resolution on the z coordinate depends on z and is in average slightly worse than the one in $R\phi$. The primary vertex of the e^+e^- interaction was reconstructed on an event-by-event basis using a beam spot constraint. The position of the primary vertex could be determined in this way with an average precision of about $40\mu m$ (slightly dependent on the flavour of the primary quark-antiquark pair) in the plane transverse to the beam direction. Secondary vertices from B semileptonic decays were reconstructed with high efficiency employing the algorithm described in [16]. The decay length resolution for the present analysis was $\sim$ 400 μm.
Leptons were identified among all the charged particles of momentum $2 < p < 30$ GeV/c. To allow the reconstruction of the $\bar{B}_d^0$ decay point only particles with at least one hit in the VD were used.

Electron identification was based on a neural network algorithm, properly combining the information from the ionisation signal in the TPC, from the energy release in the electromagnetic calorimeters, and, for tracks with momentum below 3 GeV/c from the Ring Imaging CHerenkov counters. A level of tagging providing $\sim 75\%$ efficiency within the calorimeter acceptance was chosen. The probability for a hadron to fake an electron was about one percent. Electrons from photon conversions are mainly produced in the outer ID wall and in the inner TPC frame. About 80 % of them were removed with negligible loss of signal by reconstructing the materialisation vertex.

Muons were selected by matching the track reconstructed in the tracking system to the track elements provided by the Barrel and Forward muon chambers. The efficiency was $\sim$ 80 % for $\sim$ 1 % hadron faking probability.

The experimental efficiencies and hadron faking probabilities were measured year by year using dedicated samples of leptons and hadrons independently tagged, as described in [17]; the simulation was tuned consequently.

3 Hadronic Event Selection and Simulation

Tracks from charged particles were required to have a momentum in the range $0.25 < p < 45$ GeV/c, a relative error on the momentum measurement less than 100 %, a distance of closest approach to the interaction point below 10 cm in $R\phi$ and 25 along z, a polar angle such that $|\cos(\theta)| < 0.937$. Electromagnetic showers non associated to charged tracks were required to be well contained within the calorimeter acceptance and to have an energy release greater than 0.5 (0.3) GeV in the barrel (forward) electomagnetic calorimeter. Only hadronic showers with an energy release greater than 1 GeV and not associated to tracks from charged particles were used.

The following run selection was applied: the TPC must be fully efficient, at least 95 % of the electromagnetic calorimeters and 90 % of the muon chambers had to be active. Hadronic Z decays were selected with 95 % efficiency and negligible background by using standard cuts (see [15]).

Each event was separated into two opposite hemispheres by a plane orthogonal to the thrust axis. To ensure that the event was well contained inside the fiducial volume of the detector, the cut $|\cos(\theta)| < 0.95$ was applied to the polar angle of the thrust axis of the event. Tracks were bundled into jets by using the LUCLUS [18] algorithm with default resolution parameter, $djoin = 2.5$.

About three million events were selected from the full LEP I data sets. The JETSET 7.3 Parton Shower [18] program was used to generate hadronic Z decays, which were followed through the detailed detector simulation DELSIM [19] and finally processed by the same analysis chain as the data. A sample of about seven million $Z \rightarrow q\bar{q}$ events were used. To increase the statistical significance of the simulation, a further sample of about 2.2 million $Z \rightarrow b\bar{b}$ was analysed, corresponding to about ten million equivalent Z decays. Details on the Z samples employed are reported in Table (1).

Year	data	$Z \rightarrow q\bar{q}$	$Z \rightarrow b\bar{b}$
1992+1993	1203982	2012615	922764
1994+1995	1832082	5190586	1321384
Total	3036064	7203201	2244148

Table 1: Available statistics. During years 1992 and 1993 only two-dimensional vertex reconstruction was available.

4 The $D^{*+}\ \ell^-$ sample

4.1 Event Selection

Only events containing at least one lepton candidate were further considered. The transverse momentum of the lepton relative to the jet it belonged to, p_t^ℓ, was computed after removing the lepton from the jet. The cut $p_t^\ell > 1$ GeV/c was imposed to reduce the background.

A charm hadron candidate was reconstructed from all the particles in the jet containing

the lepton, except the lepton itself, by means of the iterative algorhitm described in detail in [13, 16]. Small clusters were first formed out of the charged particles and, when possible, a decay vertex was computed for each cluster. The charm candidate so obtained was intersected with the lepton trajectory to provide the $\bar{B}^0_d$ secondary vertex; in case only one charged particle with hits in the VD belonged to the cluster, its intersection with the lepton track was computed. The cluster associated to the secondary vertex with largest statistical significance $\mathcal{S}_\mathcal{L}$ (defined as the distance from the primary vertex divided by its error; in years 1992 and 1993 only the projected distance along the $R\phi$ plane was considered) was kept as a seed. All other charged and neutral particles in the jet were ordered by decreasing values of their pseudo-rapidity relative to the cluster direction, and added to it provided the mass of the system did not exceed 2.2 GeV/c^2. The charm three-momentum was obtained from the sum of all the particles assigned to the cluster. The charm trajectory was evaluated again and was finally intersected with the lepton track to obtain the $\bar{B}^0_d$ decay point. To improve background rejection and the resolution on w (see below) events with significance $\mathcal{S}_\mathcal{L}$<4.5 were rejected.
The π^* candidate was searched for among all particles in the jet with charge opposite to the one of the lepton. If the candidate belonged to the charm cluster, the D^0 four momentum was computed after removing the π^* from the cluster and imposing the D^0 mass. To increase efficiency, also particles classified as fragmentation products were considered as π^* candidates: the D^0 was then identified with the charm cluster, constrained to the D^0 mass. D^{*+} production was finally tagged based on the mass difference Δm= M$_{D^0\pi^*}$ - M$_{D^0}$ (see Figure (1)). All events with Δm<0.165 GeV/c^2 were used for the analysis.

4.2 Event Kinematics

The variable w $(= v_{\bar{B}^0_d} \cdot v_{D^{*+}})$ can be expressed as:

$$w = (M^2_{\bar{B}^0_d} + M^2_{D^{*+}} - q^2)/(2M_{\bar{B}^0_d} M_{D^{*+}})$$

where q^2 is obtained from the $\bar{B}^0_d$ and D^{*+} four-momenta as:

$$q^2 = (p_{\bar{B}^0_d} - p_{D^{*+}})^2.$$

The D^{*+} energy, polar and azimuthal angles, and the energy of the $\bar{B}^0_d$ meson were determined as in [12]. The resolution obtained in the simulation was:

$$\begin{aligned} \sigma(E_{\bar{B}^0_d})/E_{\bar{B}^0_d} &= 10\% \\ \sigma(E_{D^{*+}})/E_{D^{*+}} &= 12\% \\ \sigma(\theta_{D^{*+}}) &= 18\ mrad \\ \sigma(\phi_{D^{*+}}) &= 21\ mrad \end{aligned}$$

The $\bar{B}^0_d$ direction was evaluated using two estimators:

- the direction obtained by inverting the vector sum of all the particles in the event except the ones assigned to the $\bar{B}^0_d$. This procedure, already used in [12], exploits three-momentum conservation in the event. The resolution depends on the hermeticity of the detector, but can also be spoiled whenever another semileptonic decay takes place in the event;

- the direction of the vector joining the primary and the secondary vertex: the resolution achieved depends on the distance between the two vertices, improving for higher values. This approach was not used in the inclusive analysis of [12].

Using the simulation, the resolution was parametrised on the basis of the missing energy in the hemisphere opposite to the $\bar{B}^0_d$ for the first estimator, and as a function of the reconstructed decay distance of the $\bar{B}^0_d$ for the second. The $\bar{B}^0_d$ meson direction was then obtained as the average of the two, weighted by the inverse of their error squared. When the difference between the two values was greater than three times its error, the direction nearest to the D^{*+} ℓ system was chosen. In the years 1992 and 1993 only the first estimator could be used to determine the $\bar{B}^0_d$ polar angle. The resolution function obtained could be parametrised by a Breit-Wigner distribution, with corresponding RMS width [‡]:

$$\begin{aligned} \sigma(\phi_{\bar{B}^0_d}) &= 18\ mrad \\ \sigma(\theta_{\bar{B}^0_d}) &= 18\ mrad \quad (1994-1995) \\ \sigma(\theta_{\bar{B}^0_d}) &= 35\ mrad \quad (1992-1993) \end{aligned}$$

The resulting w resolution function is shown by the dots in figure (2). The RMS width of the core of the distribution is approximately the same for all data sets ($\sigma(w) = 0.125$), but larger tails are present in the 1992-1993 sample due to the poorer θ measurement. The RMS width corresponds to about 25 % of the allowed kinematic range ($1 < w < 1.504$). Due to resolution effects 17.9 $\pm$ 0.4 % (32.9$\pm$0.6 %) of the events of the 94-95 (92-93) data set lay outside that range.

The squared recoil mass μ^2 was also determined on the basis of the event kinematics. It is defined as:

$$\mu^2 = M^2_{\bar{B}^0_d} + M^2_{D^{*+}\ell} - 2P_{\bar{B}^0_d} \cdot P_{D^{*+}\ell}, \tag{1}$$

where $M_{\bar{B}^0_d(D^{*+}\ell)}, P_{\bar{B}^0_d(D^{*+}\ell)}$ are the mass and four momenta of the $\bar{B}^0_d$ meson and D^{*+} ℓ system respectively. In the decay process $\bar{B}^0_d \to D^{*+}\ell^-\nu$, μ^2 represents the square of the mass of the neutrino, and should be zero; in case of background processes, due to the emission of additional particles other than the ℓ and the D^{*+} , it is usually greater than zero. This feature was exploited to determine the amount of events with intermediate D^{**} production in the sample: the measurement is discussed in section 4.4. The square recoil mass was also used to improve the w resolution: the constraint $\mu^2 = M^2_\nu (= 0\ GeV^2/c^4)$ was imposed to equation (1), which was then inverted to improve the determination of the $\bar{B}^0_d$ polar angle $\theta_{\bar{B}^0_d}$. A second order equation was obtained: the resulting ambiguity was solved by choosing the solution nearer to the previous determination. When the resolving discriminant was negative, it was forced to zero. This procedure improved the precision on the determination of w both for 1992-1993 and for 1994-1995 data samples, reducing the amount of $\bar{B}^0_d \to D^{*+}\ell^-\nu$ decays outside the allowed kinematic range to $4.8 \pm 0.1\%$. The shaded area in Figure (2) shows the w resolution finally obtained.

4.3 Determination of the Background

A set of $\mathcal{N}_t = 11353$ events was finally selected. The background consisted of the combinatorial component, due to random association of a hadron and a candidate lepton, and

[‡]RMS width defined as $\frac{F.W.H.M}{2\ log\ 2}$.

of the resonant one, due to the association of the candidate lepton to a true π^* produced by processes different from $\bar{B}^0_d \to D^{*+}\ell^-\nu$.

The combinatorial background was determined from the data, by applying the above selection to all particles in the lepton jet having the same charge as the lepton. This sample was normalised to the signal using the side mass band defined as $0.225\ \mathrm{GeV/c^2} < \Delta m < 0.3\ \mathrm{GeV/c^2}$, where the amount of events due to genuine π^* was negligible. The normalisation factor was 1.298 ± 0.013 (stat.)$\pm$ 0.021 (syst.), and the corresponding amount of combinatorial background was $\mathcal{N}_{comb.} = 4278 \pm 87$ (stat.)$\pm$89(syst.). The systematic error consisted of three contributions. The first component ($\pm$59 events) was computed by applying the same procedure to the simulated events, after having removed all events containing a genuine π^*, in order to verify that the particles with wrong charge correlation well reproduce the actual combinatorial background. The difference between the good and wrong charge samples, after normalisation, was 44 ± 59 events. The second component ($\pm$64) was due to the subtraction of a small amount of events in the wrong charge sample produced when either the lepton from D^0 semileptonic decay (84 ± 42 events) or else a fake hadron with the same charge as a true π^* (91 ± 46) were selected. The residual contribution was due to leakage of π^*events into the side band.

The total amount of D^{*+} was then $\mathcal{N}_{D^{*+}} = 7075 \pm 138 \pm 89$.

The following processes contributed to the resonant background: fake leptons randomly associated to a π^*, b decays to a D^{*+} with another heavy flavour decaying semileptonically, $b \to D^{*+}X_c/\tau^-X$ (followed by $X_c/\tau^- \to \ell X$), production of D^{**} in b semileptonic decays. The contribution from the first two sources was determined from the simulation, tuned to the most recent measurement of the relevant branching ratios (when available); the last one was measured from the data. Table (2) shows the individual contributions to the D^{*+} sample; the composition was calculated using the values of the branching ratios for all the relevant processes as reported in Table (4).

Hadrons faking a lepton can couple to D^{*+} produced either from $b\bar{b}$ or $c\bar{c}$ decays of the Z (the contribution from gluon splitting to D^{*+} is negligible). Their total amount was computed by determining independently the probability for a hadron to fake a lepton, known with $\sim \pm 5\%$ relative precision [17], and the product of branching ratios $BR(Z \to b\bar{b}(c\bar{c})) \times BR(b(c) \to D^{*+})$ [28].

The rate for the $\bar{B}^0_d \to \tau^- D^{*+}$ decay was obtained from the measurement of the inclusive BR$(b \to \tau^-\bar{\nu}_\tau X)$, assuming that a D^{*+} be produced in (70 ± 10) % of the cases.

The fraction of inclusive double charm decays $b \to D^{*+}X_c$ was determined from charm counting measurements as suggested in [25]. The error was inflated to account for the uncertainty in the inclusive semileptonic decay $X_c \to \ell\bar{\nu}X$.

The knowledge of the contamination from D^{**} intermediate states was the dominant source of systematic error in the previous analysis[12], where it was determined by inspecting the decay $B^- \to D^{*+}\ell\pi^-\bar{\nu}$: events were tagged by looking for an additional charged pion from the B^- decay point in a sample of exclusively reconstructed $D^{*+}\ \ell$ events. The fraction of events due to D^{**} intermediate production in b semileptonic decays with a D^{*+} in final state was determined as

$$\mathcal{R}^{**} = \frac{BR(b \to D^{**}\ell\nu)}{BR(b \to D^{**}\ell\nu) + BR(b \to \bar{B}^0_d \to D^{*+}\ell^-\nu)} = (19 \pm 10)\%, \qquad (2)$$

by further assuming isospin and flavour SU(3) conservation to account for $\bar{B}^0_d \to D^{*+}\ell\pi^0\bar{\nu}$

and $B_s \to D^{*+}\ell K^- \bar{\nu}$ decays respectively.[§] An independent determination of $\mathcal{R}^{**}$ has later been performed based on the inclusive D^{*+} sample described above. The measurement will be discussed in the next chapter.

4.4 Evaluation of the D^{**} fraction

Semileptonic decays from the direct process $\bar{B}^0_d \to D^{*+}\ell^-\nu$ can be distinguished from the cascade chain $b \to D^{**}\ell\nu$, $D^{**} \to D^{*+}X$ exploiting the squared recoil mass μ^2 distribution (see equation 1). The method was originally proposed by the ARGUS collaboration (see [7]): due to the additional particles produced in the decay of a D^{**} to a D^{*+}, the value of μ^2 computed as in equation (1) is greater than zero. It is therefore possible to distinguish direct from cascade decays (see Figure (3)). Resolution effects reduce the separation between the D^{*+} and the D^{**} sample. Studies based on the simulation showed that the resolution is mainly determined by the precision on the measurement of the $\bar{B}^0_d$ direction. For this reason, the analysis was limited to the data collected since 1994.

A fit was performed to the experimental μ^2 distribution, fixing the contribution from all background sources different from D^{**} to the values computed above, and leaving as free parameters the number of events from the direct (D^{*+}) process, $\mathcal{N}^*$, and from the cascade (D^{**}), $\mathcal{N}^{**}$. In the fit, the shape of the μ^2 spectra for the combinatorial background was obtained from the data, using the wrong charge sample and subtracting the small resonant contribution (see above). The same result was obtained when using instead the shape predicted from the simulation; a Kolmogorov test, comparing the distributions for the good and wrong charge combinatorial background in the simulation, gave ~ 60 % probability. The shape of the μ^2 distribution for $D^{**}$was computed after reweigthing the simulated w spectra to the predictions of HQET (see [21]), and properly accounting for the systematic error due to the choice of the model. $\bar{B}^0_d \to D^{*+}\ell^-\nu$ decays were described using the IGSW model [22]; events were then reweighted to account for different parametrisations, but no appreciable effect on the result was observed. The shape of the μ^2 distribution for all other sources was taken from the simulation.

The value of $\mathcal{R}^{**}$was then obtained by correcting r^{**} for the different efficiencies to observe D^{*+} and D^{**}events:

$$\mathcal{R}^{**} = \frac{\mathcal{N}^{**}/\epsilon^{**}}{\mathcal{N}^{**}/\epsilon^{**} + \mathcal{N}^{*}/\epsilon^{*}} = \frac{r^{**}}{r^{**} + (1 - r^{**})\frac{\epsilon^{**}}{\epsilon^{*}}} = 0.18 \pm 0.11(stat.) \pm 0.05(syst.) \qquad (3)$$

where $\epsilon^* = 14.7 \pm 0.1\%$ ($\epsilon^{**} = 9.5 \pm 0.1\%$) is the efficiency to reconstruct $\bar{B}^0_d \to D^{*+}\ell^-\nu$ ($b \to D^{**}\ell\nu$) decays. The systematic error will be discussed in detail in chapter 6.

The two results 2 and 3 are mutually consistent and independent, because they were obtained with different techniques on uncorrelated data samples. Their average value was computed as:

$$\mathcal{R}^{**} = (19 \pm 8)\% \qquad (4)$$

[§]A more precise measurement based on the same approach has recently been performed, yielding $\mathcal{R}^{**} = 0.27 \pm 0.05$ (see [20]). The correspondent preliminary value of $\mathcal{R} = 0.29 \pm 0.06$ is found, consistent with the number quoted above.

Source	Amount (I)	Amount (II)
Data	11353	10232
Combinatorial	4278±87	3756±81
$\bar{B^0_d} \to D^{*+}\tau\bar{\nu}$	121±4	73±4
$b \to D^{*+}X_c$	97±4	74±4
fake leptons	282±8	245±8
$b \to D^{**}\ell^-\bar{\nu}$	878 ± 10	769 ± 10
$\bar{B^0_d} \to D^{*+}\ell^-\nu$	5697±88	5315±82

Table 2: Composition of the sample used for the analysis, before (I) and after (II) the cut on μ^2, quoted errors are only of statistical origin.

4.5 Final Selection and Sample Composition

The relative fraction of $D^{**}$and D^{*+} events in the simulation was then fixed to the value obtained above, see equation (4). Events with μ^2 greater than 2 GeV^2/c^4 were rejected to reduce the D^{**}contamination. The composition of the final sample is reported in the last column of Table (2). The constraint μ^2= 0 GeV^2/c^4 was then imposed to each selected event to compute the value of w with the best possible accuracy (see section 4.2).

5 Determination of $|V_{cb}|$

5.1 Parametrisation of the Decay Width

The expected amount of signal events can be expressed as a function of w by the relation:

$$\begin{aligned} d\mathcal{N}/dw &= 4\ N_Z\ R_b\ f_d\ Br(\pi^*)\ \epsilon(w)\ d\Gamma/dw, \\ d\Gamma/dw &= \frac{G_F^2}{48\pi^3\hbar\ \tau_{\bar{B^0_d}}} M^3_{D^{*+}}(M_{\bar{B^0_d}} - M_{D^{*+}})^2\ \sqrt{w^2-1}\ (w+1)^2 \\ &\times\ |\ V_{cb}\ |^2\ \ \mathcal{F}^2(w) \left[1 + \frac{4w}{1+w}\frac{1-2wr+r^2}{(1-r)^2}\right] \end{aligned} \tag{5}$$

The factor 4 accounts for the fact that a $\bar{B^0_d}$ can be produced in either hemispheres, and that both electrons and muons were used; N_Z is the number of hadronic events, R_b the fraction of hadronic Z decays to a $b\bar{b}$ pair, f_d the probability for a b quark to hadronize into a $\bar{B^0_d}$ meson, $Br(\pi^*)$ the branching ratio for the decay $D^{*+} \to D^0\pi^+$, $\tau_{\bar{B^0_d}}$ the $\bar{B^0_d}$ lifetime and r is the ratio of meson masses, $r = M_{D^{*+}}/M_{\bar{B^0_d}}$. The values employed for these parameters, as determined by independent measurements, are reported in Table (4). The quantity $\epsilon(w)$, product of the acceptance and of the reconstruction efficiency (which exhibits a slight dependence on w), was instead determined on the basis of the tuned simulation.

The analytical expression of the form factor $\mathcal{F}(w)$ is unknown. Due to the small w range allowed by phase space, a Taylor series expansion limited to second order was used in the past:

$$\mathcal{F}(w) = \mathcal{F}(1)\ (1 + \rho^2_{\mathcal{F}}(1-w) + c(1-w)^2 + \mathcal{O}(1-w)^3). \tag{6}$$

Contrary to $\mathcal{F}(1)$, the theory does not predict the values of the higher order coefficients, which must be determined experimentally. First measurements of $|V_{cb}|$ were performed assuming a linear expansion, i.e. neglecting second order terms ([7, 8, 9, 12]). Basic considerations derived from the request of analyticity and positivity of the QCD functions describing the local currents predict however that a positive curvature coefficient c should be expected, which must be related to the radius of the heavy meson $\rho^2_{\mathcal{F}}$(see [5]) by the relation:

$$c \;=\; 0.66\rho^2_{\mathcal{F}} - 0.11 \tag{7}$$

Results exploiting the above analyticity bound were derived by the ALEPH and OPAL collaborations (see [10, 11]). An improved parametrisation based on the above consideration was recently proposed (see [6]): it accounts for higher order terms, so reducing to $\pm 2\%$ (according to the authors) the relative uncertainty on $|V_{cb}|$ due to the form factor parametrisation. A novel function $\mathcal{A}_1(w\,)$ was introduced, connected to $\mathcal{F}(w\,)$ by the following relation:

$$\begin{aligned} \mathcal{F}^2(w) \quad &\times \quad \left[1 + \frac{4w}{1+w}\frac{1-2wr+r^2}{(1-r)^2}\right] \;= \\ \mathcal{A}_1^2(w) \quad &\times \quad \left\{2\frac{1-2wr+r^2}{(1-r)^2}\left[1+\frac{w-1}{w+1}R_1(w)^2\right] + \left[1+\frac{w-1}{1-r}(1-R_2(w))\right]^2\right\} \end{aligned} \tag{8}$$

where $R_1(w\,)$ and $R_2(w\,)$ are ratios of axial and vector form factors; their analytical expressions can be found in [6]. The following parametrisation, depending only on a single unknown parameter $\rho^2_{\mathcal{A}_1}$, was obtained for $\mathcal{A}_1(w\,)$:

$$\mathcal{A}_1(w) \;=\; \mathcal{A}_1(1)\left[1 - 8\rho^2_{\mathcal{A}_1}z + (53\rho^2_{\mathcal{A}_1} - 15)z^2 - (231\rho^2_{\mathcal{A}_1} - 91)z^3\right]$$

with

$$z = \frac{\sqrt{w+1} - \sqrt{2}}{\sqrt{w+1} + \sqrt{2}}$$

It should be noted that, in the limit $w \to 1$, $\mathcal{A}_1(w\,) \to \mathcal{F}(w\,)$, so that $\mathcal{A}_1(1) \approx \mathcal{F}(1)$.

Experimental data were fitted using this last parametrisation and results were also obtained with older forms for sake of comparison.

5.2 Fit to the Experimental Data

Real and simulated data were collected in several w bins of variable size. A minimum χ^2 fit was then performed comparing the numbers of observed and expected events in each bin. The normalisation of the background was determined as explained above. The shape of the w distribution for the combinatorial was obtained from the wrong charge data, simulated D^{**} spectra were corrected to reproduce the predictions of [21], the spectra for all the other background sources were taken from the simulation. The contribution from the signal was obtained at each step of the minimisation by properly weighting each generated event surviving the selection; for a given value of w the weight was equal to the ratio between the value taken by the fitting function and the one of the generation function, which was parametrised as in equations (6,6), with $\rho^{2\,gen}_{\mathcal{F}} = 0.8151$ and $c^{gen} = 0$.

Using the parametrisation of equation (8) the following set of results was obtained:

$$\begin{aligned} \mathcal{A}_1(1) \mid V_{cb} \mid &= (37.95 \pm 1.34) \times 10^{-3} \\ \rho^2_{\mathcal{A}_1} &= 1.39 \pm 0.12 \\ BR(\bar{B}^0_d \to D^{*+}\ell^-\nu) &= (5.22 \pm 0.12)\% \end{aligned}$$

where the last quantity was obtained from integration of the differential decay width. The correlation between the two fitted parameters was 0.94. Figure (4) shows the comparison between the data and the result of the fit.

It should be noted that the fit was performed separately on 1992-1993 and 1994-1995 data sets, and then the results have been averaged. Individual results obtained with the two data sets are in agreement, as can be seen in Table (3).

Fit Method (sample)	$\mid \mid V_{cb} \mid \mid \mathcal{A}_1(1) \times 10^3$	$\rho^2_{\mathcal{A}_1}$	$\rho^2_{\mathcal{F}}$	c
Eq. (8) 92-93	38.83 ± 2.32	1.39 ± 0.21	-	-
Eq. (8) 94-95	37.55 ± 1.64	1.39 ± 0.15	-	-
Eq. (8) 92-95	37.95 ± 1.34	1.39 ± 0.12	-	-
Eq. (7) 92-95	37.88 ± 1.39	-	1.14 ± 0.13	$0.66\rho^2_{\mathcal{F}}$-0.11
Eq. (6) 92-95	37.97 ± 1.71	-	1.17 ± 0.38	0.77 ± 0.91
Linear 92-95	36.69 ± 1.22	-	0.83 ± 0.10	0
Linear 94 only	36.39 ± 1.52	-	0.84 ± 0.12	0

Table 3: Results of different fits to the experimental data

The same Table contains also the results obtained when using the other parametrisations of form factors discussed previously. In detail, the Taylor expansion of equation (6) was employed, by either assuming a linear expansion (c=0), or else imposing to the curvature c the constraint of equation (7), and by finally fitting $\rho^2_{\mathcal{F}}$ and c as independent free parameters. In this last case, the correlation coefficients with $|V_{cb}|\mathcal{F}(1)$ were 0.82 and 0.71 respectively, the mutual correlation was 0.97. To verify the consistency with the published result of [12], obtained by assuming a linear expansion and exploiting only 1994 data, this result is reported as well.

6 Systematic Errors

Uncertainties in the overall normalisation, in the knowledge of the selection efficiency and of the composition of the sample, including the modelling of the background, and about the matching between the experimental resolution and the simulated one may affect the result. They were all considered as sources of systematic error.

The fit was performed several times, by varying in turn all the parameters which determine the normalisation (see equation (6)) within the allowed range (see Table (4)); the corresponding variations of the measured quantities were added quadratically to the systematic error.

The efficiency depends on the detector performances in tracking reconstruction, lepton identification and secondary vertex reconstruction.

Tracks from charged particles may either be lost due to cracks in the tracking device, or else due to hard scattering of the particle with the detector frames. Electrons and low momentum $\pi^*$are more sensitive to this last effect. A conservative error of $\pm 1\%$ per track was assigned based on studies of the detector material (performed using electrons from photon conversion) and of the TPC cracks.
As already mentioned, the actual efficiency for lepton identification was measured exploiting samples of data tagged independently. Muons from τ decays and from the process $\gamma\gamma \rightarrow \mu^+\mu^-$ allowed to explore all the interesting kinematic range. The values of the experimental and predicted efficiencies were consistent within $\pm 2\%$. Electrons from photon conversion and from the radiative Bhabha process were also used. Compared to the simulation, a relative inefficiency of $(94 \pm 2)\%$ was found, where the error is due to the systematic difference between the two samples. This ratio does not depend on the particle momentum.
To provide an accurate description of the algorithm employed for vertex reconstruction, the simulation was tuned following the procedure of [23], developed for the precise measurement of R_b. The efficiency was then determined by comparing in the data and in the simulation the fraction of vertices reconstructed in a sample of high momentum leptons. The relative efficiency was 1.01 ± 0.01.

Due to the cuts on the lepton momentum p and decay length significance $\mathcal{S}_\mathcal{L}$ (see section 4.1) the efficiency depends on the average fraction of the beam energy actually carried by the $\bar{B}^0_d$ meson, $< x_E >$. Events were generated assuming the Peterson fragmentation function ([24]), tuned so as to reproduce the measured value of $< x_E > \; = \; 0.702 \pm 0.008$ [25]; they were then reweighted in the fit in order to allow $\pm$ 0.008 variation on $< x_E >$, and the consequent variation on the fitted parameters was propagated into the errors.
Model dependent uncertainties may be introduced by the kinematic cuts on p_t^ℓ and μ^2 as well. They were determined following the iterative procedure applied in [12]: the simulated spectrum was corrected to the measured values and the efficiency computed again. The efficiency varied by ~ 1 %. This was taken as the systematic error, and no further iteration was performed.

Each source of background was varied by its error as reported in Table (2) and the variation of the results was propagated into the error. The uncertainty due to the description of D^{**} production and decay was determined by adding quadratically two contributions: first the slope of the corresponding form factor $\mathcal{F}_{D^{**}}$ was varied by $\pm 50\%$; then the fraction of resonant states in the D^{**} sample was varied between 0 and 100 %.

All quantities relevant to the determination of the w resolution were inspected. Agreement was found between the distributions of the D^{*+} energy in the data and in the simulation; the angular resolution on the D^{*+} direction was checked by comparing the relative angle between the π^* and the D^0 directions and again optimal agreement was found.
The estimate of the $\bar{B}^0_d$ energy depends on the hermeticity of the detector. To verify that cracks were properly simulated, a sample of b enriched events was provided by b-tagging one hemisphere and analysing the other (unbiased). Only hemispheres without identified leptons were considered, in order to avoid possible distorsions due to the presence of a neutrino. The procedure was applied to the data and to the simulation, and the visible energy was compared in the two cases. Depending on the year, the energy seen in the data (~ 37 GeV) exceeded the one predicted by about 400 MeV. The main source of discrepancy was attributed to the tracking. Due to the smallness of the effect, no further investigation

was performed but two different correction procedures were followed: either the visible energy in the simulation was increased by a proper amount, or else a correction was computed depending on the fraction of charged energy seen in the event. The systematic error was chosen as the maximum difference between the result so obtained and the one without fine tuning.
The $\bar{B}^0_d$ angular resolution was compared in the data and in the simulation by inspecting the angle between the $\bar{B}^0_d$ and the D^{*+} ℓ directions. The RMS widths of the two distributions were identical within errors (42.5±0.6 and 42.6± 0.6 mrad respectively). The systematic error on $|V_{cb}|$was computed by repeating the fit without the μ^2constraint.

The systematic error induced by the fitting procedure applied was determined by varying the number of bins and their size, by eventually removing the (few) events outside the physically allowed w region. The effect of the other cuts applied in the analysis was checked by varying them in the ranges :

- the Δm cut between 0.15 and 0.18 GeV/c^2,
- the p_t^ℓ cut between 0.8 and 1.25 GeV/c,
- the μ^2 cut between 0. and 5. GeV^2/c^4 (for the $|V_{cb}|$ fit only),
- the $\mathcal{S}_\mathcal{L}$ cut between 2.5 and 6.5

It should be noted that the efficiency and purity of the sample vary by more than 50 % in the above ranges, and most of the induced variations are compatible with statistical fluctuations. They were conservatively assumed as systematic errors. For further check the analysis was performed separately for electrons and muons. Excellent agreement was found. All the errors discussed above were added in quadrature to determine the final systematic error. Their individual contribution is reported in Table (4).

7 Extraction of the form factor

The result discussed above was obtained in the frame of a specific model. It is in principle possible to extract the differential decay width, $\frac{d\Gamma}{dw}$ and the Isgur Wise function $\mathcal{A}(w)$ from the experimental data. To cope with the non negligibile smearing due to the experimental resolution, an unfolding procedure was applied [29, 30].

The simulated events which survived the selection were first grouped in ten bins, according to the value of w_{gen} at generation. Due to the finite experimental resolution, events lying in the same bin in w_{gen} populated several bins in the reconstructed w_{rec} distribution. Per each w_{gen} bin, a corresponding w_{rec} histogram was therefore obtained. To overconstrain the fit, the new histograms consisted of twelve bins. The linear combination of these ten histograms was fitted to the data distribution. The ten parameters of the fit determined the normalisation coefficients of each simulation histogram. The unfolded differential decay width was finally obtained by binning all the simulated events according to their w_{gen}, and scaling the resulting histograms with the fitted parameters.

To avoid spurious bin to bin oscillations, typical of such an unfolding method, a regularisation term was added to the χ^2, proportional to the second derivative of the unfolded results:

$$\chi^2_{reg} \quad = \quad \tau \cdot \Sigma_{i=2}^{n-1} |(f_{i+1} - f_i) - (f_i - f_{i-1})|^2$$

$$\approx \quad \tau \cdot \int |f''(x)|^2 dx$$

The regularisation parameter τ is in principle arbitrary. Too small values lead to oscillating solutions, whereas large values produce flat solutions, with small errors and strong positive correlations among parameters. Several fits were performed, with τ ranging from 0.01 to 1.0: to test the method, the unfolded distributions were fitted with the function of equation 8 neglecting bin to bin correlations. The values obtained for $\mathcal{A}_1 \cdot |V_{cb}|$and $\rho^2_{\mathcal{A}_1}$were always well compatible with the ones of section 5, but their errors depend on the choice of τ (lower values leading to higher errors). Choosing τ=0.20 the same errors as the ones of section 5 were obtained. The corresponding spectra are presented in Figures (5 a,b), where the proper function (dotted line) and the one obtained by fitting directly the histogram (continuous line) are overlayed to the unfolded spectra.

To remove the sensitivity of the errors in the choice of τ, fits were finally performed properly accounting for bin to bin correlations. The result was:

$$\begin{aligned} \mathcal{A}_1 \cdot |V_{cb}| &= (37.73 \pm 1.38) \times 10^{-3} \\ \rho^2_{\mathcal{A}_1} &= 1.38 \pm 0.13 \end{aligned}$$

independently of the choice of τ. The values of the unfolded data points and of their covariance matrix are given in Table (5)

8 Conclusions

A sample of about 5500 $\bar{B^0_d} \to D^{*+}\ell^-\nu$ decays was obtained by means of the method of the inclusive π^* tagging, originally developed at LEP by the DELPHI collaboration. The use of the large data set, and the excellent detector performance allowed the precise measurement of the product $|V_{cb}|\cdot\mathcal{A}_1(1)$ and of the $\bar{B^0_d}$ radius $\rho^2_{\mathcal{A}_1}$, following the most recent parametrisation of the Isgur-Wise function as proposed in [6]:

$$\begin{aligned} \mid V_{cb} \mid \cdot \mathcal{A}_1(1) &= (37.95 \pm 1.34(stat.) \pm 1.59(syst.)) \times 10^{-3} \\ \rho^2_{\mathcal{A}_1} &= 1.39 \pm 0.12(stat.) \pm 0.18(syst.) \end{aligned}$$

Using the value $\mathcal{A}_1(1) \approx \mathcal{F}(1) = 0.91 \pm 0.03$ the following value of $|V_{cb}|$is obtained:

$$\mid V_{cb} \mid \;=\; (41.70 \pm 1.47(stat.) \pm 1.74(syst.\ exp.) \pm 1.38(syst.\ th)) \times 10^{-3}$$

This result replaces the previous DELPHI measurement of [12].
The value of the branching ratio for the decay $\bar{B^0_d} \to D^{*+}\ell^-\nu$ was determined by integration as:

$$Br(\bar{B^0_d} \to D^{*+}\ell^-\nu) \;=\; (5.22 \pm 0.12 \pm 0.55)\%$$

The analysis of the event kinematics allowed also to determine the relative production fraction of orbitally excited D mesons decaying to a D^{*+} as:

$$\mathcal{R}^{**} = \frac{BR(b \to D^{**}\ell\nu, D^{**} \to D^{*+}X)}{BR(b \to D^{*+}\ell\bar{\nu}X')} = (18 \pm 11(stat.) \pm 5(syst.))\%,$$

which averaged to the previous DELPHI measurement published in [12] gives:

$$\mathcal{R}^{**} = (19 \pm 8)\%.$$

By properly accounting for the correlations between $\mathcal{R}$ and the BR($\bar{B}_d^0 \to D^{*+}\ell^-\nu$) the other two values were finally obtained:

$$\begin{aligned} BR(b \to D^{*+}\ell\bar{\nu}X) &= (2.55 \pm 0.21)\% \\ BR(b \to D^{**}\ell\bar{\nu}, D^{**} \to D^{*+}X) &= (0.48 \pm 0.22)\% \end{aligned}$$

9 Acknowledgments

We are greatly indebted to our technical collaborators and to the funding agencies for their support in building and operating the DELPHI detector, and to the members of the CERN-SL Division for the excellent performance of the LEP collider.

References

[1] P.Paganini,F.Parodi,P.Roudeau,A.Stocchi hep-ph/9711261;
F.Parodi,P.Roudeau,A.Stocchi hep-ph/9802289.

[2] M.A.Shifman and M.B.Voloshin, Sov.J.Nucl.Phys. **47** (1988) 511;
N.Isgur and M.Wise, Phys.Lett. **237** (1990) 527;
A.F.Falk,H.Georgi,B.Grinstein and M.B.Wise, Nucl,Phys, **B 343** (1990) 1;
M.Neubert, Phys.Lett. **B 264** (1991) 455;
M.Neubert, Phys.Lett. **B 338** (1994) 84.

[3] A.Czarnecki,Phys.Rev.Lett.**76** (1996) 4126.

[4] A.F.Falk, M.Neubert , Phys.Rev.**D 47**(1993) 2965 and 2982;
T.Mannel, Phys. Rev. **D 50** (1994) 428;
M.A.Shifman N.G.Uraltsev and M.B.Voloshin, Phys.Rev. **D 51** (1995) 2217.

[5] I.Caprini, M.Neubert, Phys.Lett. **B 380** (1996) 376.

[6] I.Caprini, L.Lellouch, M.Neubert,
'Dispersive Bounds on the Shape of $\bar{B} \to D^{(*)}\ell\bar{\nu}$ Form Factors'
CERN-TH/97-91, hep-ph/9712417;
C.G.Boyd, B.Grinstein, R.F.Lebed,Phys.Rev. **D 56** (1997) 6895.

[7] H.Albrecht et al. (ARGUS *coll*), Z.Phys. **C 57** (1993) 533.

[8] B.Barish et al. (CLEO *coll*), Phys.Rev. **D 51** (1995) 1014.

[9] B.Buskulic et al. (ALEPH *coll*), Phys.Lett **B 359** (1995) 236.

[10] B.Buskulic et al. (ALEPH *coll*), Phys.Lett **B 395** (1997) 373.

[11] K.Ackerstaff et al. (OPAL *coll*), Phys.Lett B **B 395** (1997) 128.

[12] P.Abreu et al.(DELPHI *coll*), Z.Phys.**C 71** (1996) 539.

[13] P.Abreu et al.(DELPHI *coll*), Z.Phys.**C 74** (1997) 19.

[14] P.Abreu et al.(DELPHI *coll*), Z.Phys.**C 76** (1997) 579.

[15] P.Abreu et al.(DELPHI *coll*), Nucl. Instr. and Meth. **A378** (1996) 57

[16] P.Paganini Ph.D. Thesis LAL 96-18 , May 96.

[17] F.Stichelbaut, G.Wilkinson, DELPHI internal note 97-37 Phys. 690;
G.Wilkinson, DELPHI internal note 95-140 Phys. 565;
K.D. Brand, I. Roncagliolo, F. Simonetto, DELPHI internal note 96-23 PHYS 598;
see also the WEB page http://delphi.pd.infn.it/ margoni/lepid/

[18] T.Sjöstrand, Comp. Phys. Comm. **82** (1994) 74.

[19] P.Abreu et al.(DELPHI *coll*), Nucl. Instr. and Meth. **A378** (1996) 57

[20] D.Bloch,P.Julliot,P.Roudeau,R.Strub

'Measurement of the B semileptonic Branching Fraction into Orbitally Excited Charm Mesons'

DELPHI internal note 99-103 CONF 290; contribution number 5_514 to this conference; contributed paper 239 to the XXIX International Conference on High Energy Physics, Vancouver July 23-29 , 1998

[21] V.Morenas, A.Le Yaouanc, L.Oliver, O.Pene and J.-C.Rayal

Quantitative Predictions for B semileptonic decays into D, D^* and the orbitally excited D^{**} in quark models la Bakamjian-Thomas .

LPTHE Orsay-97/19 PCCF RI 9707 hep-ph/9706265

[22] N.Isgur and M.Wise, Phys.Lett. **232** (1989) 113.

[23] G.V. Borisov and C. Mariotti, Nucl.Instr. and Method **A372** (1996) 181.

[24] C.Peterson et al., Phys.Rev, **D 27** (1983) 105.

[25] The LEP collaborations, ALEPH,DELPHI,L3,OPAL, the LEP Electro-weak Working Group and the SLD Heavy Flavour and Electroweak Working groups, "A Combination of Preliminary Electroweak Measurements and Constraints on the Standard Model",preprint CERN-EP/99-15, Geneva 1999.

[26] The Particle Data Group, Eur. Phys. J. C3 (1998) 1;

also on the WEB page http://www-pdg.lbl.gov/

[27] The LEP B oscillations working group, "Combined Results on $\bar{B}^0_d$ oscillations: Results from Winter 1999 Conferences", LEPBOSC 99/1.

[28] P.Abreau et al.(DELPHI *coll*), "Measurements of the Z Partial Decay Width into $c\bar{c}$ and Multiplicity of Charm Quarks per b Decay " CERN-EP/99-66, submitted to Eur.Phys. J.C.

[29] V.Blobel, "Unfolding in High Energy Physics",

Procs. CERN School of Computing, Aiguablava (Spain),

CERN,Geneva,1985,p.88.

[30] G.Zech,"Comparing Statistical Data to Monte Carlo Simulation",

DESY prep. 95-113

Parameter	Value	$\frac{\Delta(R^{**})}{R^{**}}$ %	$\frac{\Delta(\lvert V_{cb}\rvert)}{\lvert V_{cb}\rvert}$ %	$\Delta\ (\rho^2_{\mathcal{A}_1})$	$\frac{\Delta(Br)}{Br}$ %
R_b	$(21.66 \pm 0.07)\%$ [25]	-	0.25	-	0.5
$\mathcal{B}(D^{*+} \to D^0\pi^+)$	$(68.3 \pm 1.4)\%$ [26]	0.5	1.20	0.01	2.5
$\mathcal{B}(\bar{B^0_d} \to D^{*+}\ \tau^-\bar{\nu})$	$(1.82 \pm 0.38)\%$ [25]	13.8	0.23	-	0.19
$\mathcal{B}(D^0 \to \ell^+\nu X)$	$(6.75 \pm 0.29)\%$ [26]	1.6	0.10	-	-
$\mathcal{B}(b \to D^{*+}X)$	$(23.1 \pm 1.3)\%$ [28]	0.5	0.05	-	0.19
$\mathcal{B}(c \to D^{*+}X)$	$(24.0 \pm 1.3)\%$ [28]	0.5	0.13	-	-
$\mathcal{B}(b \to D^{*+}X_c,$ $X_c \to \ell^-\bar{\nu}X)$	$(1.22^{+0.33}_{-0.27})\%$[25]	10.9	0.15	0.01	0.30
$f_d = \mathcal{B}(b \to B^0_d)$	$(39.5 \pm 1.4)\%$ [27]	2.7	2.10	0.02	3.50
$f_s = \mathcal{B}(b \to B_s)$	$(10.5 \pm 1.8)\%$ [26]	2.2	0.16	-	0.40
$f_\Lambda = \mathcal{B}(b \to \Lambda_b)$	$(10.1 \pm 3.5)\%$[26]	4.9	0.13	-	0.40
$\tau_{\bar{B^0_d}}$	$(1.56 \pm 0.04)ps$[26]	2.2	1.63	-	0.99
τ_{B^+}	$(1.65 \pm 0.04)ps$[26]	0.5	0.03	-	0.20
τ_{B_s}	$(1.54 \pm 0.07)ps$[26]	-	0.03	-	0.20
τ_{Λ_b}	$(1.24 \pm 0.08)ps$[26]	-	-	-	-
Tracking		-	1.00	-	2.00
II Vertex		-	0.50	-	1.00
ℓ eff. & bck.		1.6	0.7	-	1.50
Combinatorial		4.3	0.52	0.02	1.87
E_ν tuning		16.3	0.21	0.01	0.19
D^{**} slope		0.5	0.65	0.03	0.56
D^{**} decay		6.5	0.70	0.05	1.50
D^{**} fraction		-	0.99	0.12	8.65
fragmentation		1.0	0.99	-	1.90
fit		-	0.23	0.02	0.20
$\mathcal{S}_\mathcal{L}$vertex	2.5-6.5	-	$^{+.60}_{-1.00}$	$^{+0.01}_{-0.07}$	$^{+1.60}_{-0.10}$
P_t lepton	0.8-1.25 (GeV/c)	-	$^{+0.02}_{-.50}$	-0.04	+0.80
Δm	0.15-0.18(GeV/c^2)	-	$^{+1.80}_{-1.10}$	$^{+0.11}_{-0.03}$	2.70
μ^2	0.0-5.0 (GeV^2/c^4	-	$^{+1.30}_{-0.70}$	$^{+0.05}_{-0.02}$	$^{+2.40}_{-0.30}$
resolution	no μ^2constrain	-	-2.10	-0.07	-0.50
sum		$\pm$26.0	$\pm$4.2	$\pm$0.18	$\pm$10.50

Table 4: Contributions to the systematic errors. The values used for the parameters relevant to this analysis are reported in the second column. Errors for $|V_{cb}|$ and Br are relative and given in %, for the other quantities the errors are absolute.

$< w >$-1	.025	.075	.125	.175	.225	.275	.325	.375	.425	.477
$\frac{d\Gamma}{dw}$	3.41	5.77	6.64	6.82	6.62	6.15	5.72	5.39	4.81	3.88
	.336	.126	-.138	-.210	-.140	-.029	.043	.065	.052	.029
		.250	.102	-.082	-.163	-.134	-.061	.010	.059	.080
			.397	.235	-.032	-.186	-.188	-.101	.012	.094
				.491	.249	-.052	-.197	-.186	-.089	.006
					.501	.269	-.005	-.163	-.203	-.180
						.526	.307	.003	-.234	-.349
							.495	.232	-.121	-.359
								.354	.113	-.129
									.334	.319
										.738

Table 5: The unfolded differential decay width. First line: w bin centre. Second line: value of the function (multiplied by 10^3). Other lines: error matrix (values multiplied by 10^6).

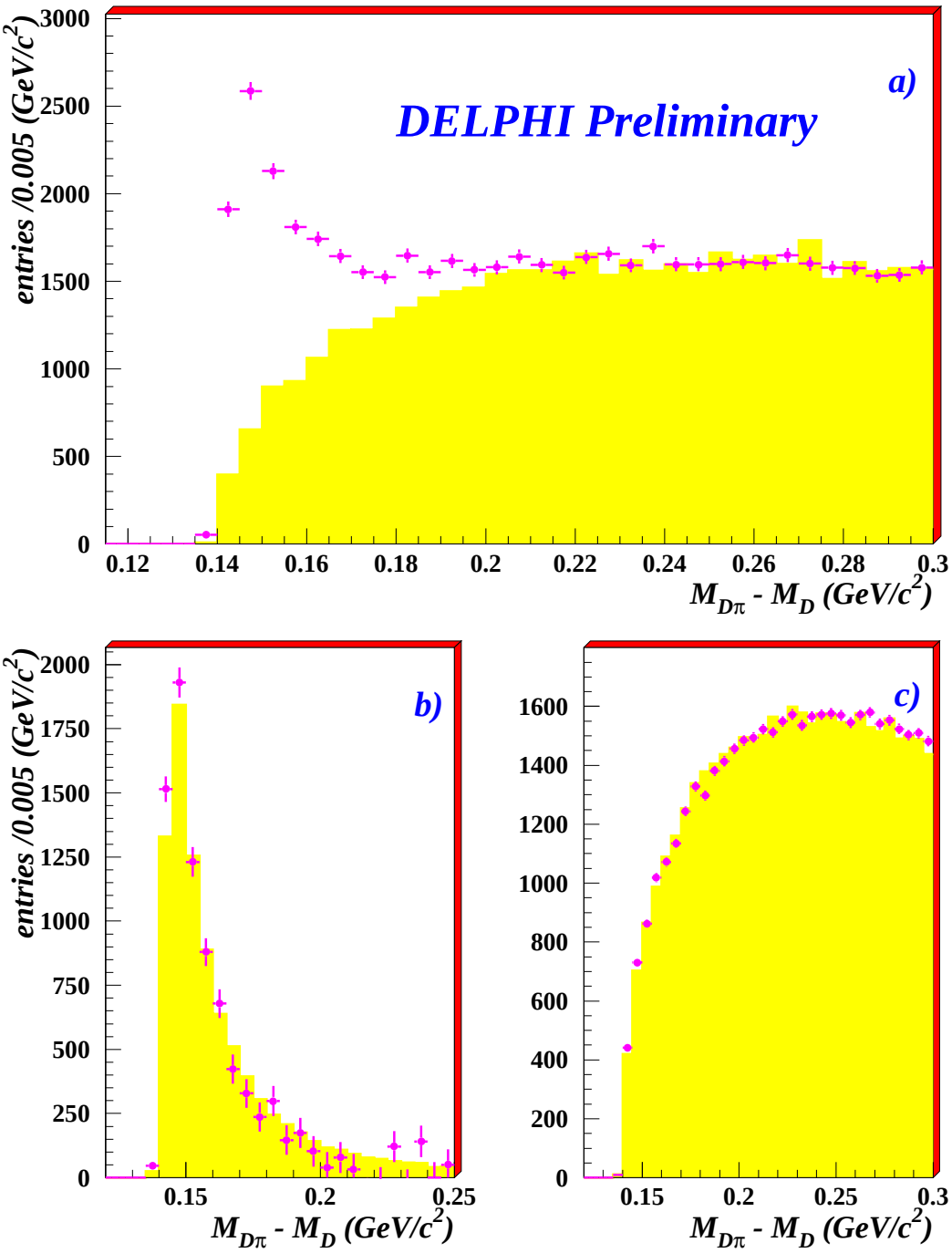

Figure 1: Mass difference: $M_{D\pi} - M_D$.
a) opposite charge, data (crosses), same charge (shaded area), normalised in the side band defined in the text
b) opposite charge , data after subtraction of the combinatorial background (crosses), resonant contribution from simulation (shaded area), with arbitrary normalisation
c) simulation: combinatorial from opposite charge (crosses), compared to the equal charge combination normalised in the side band

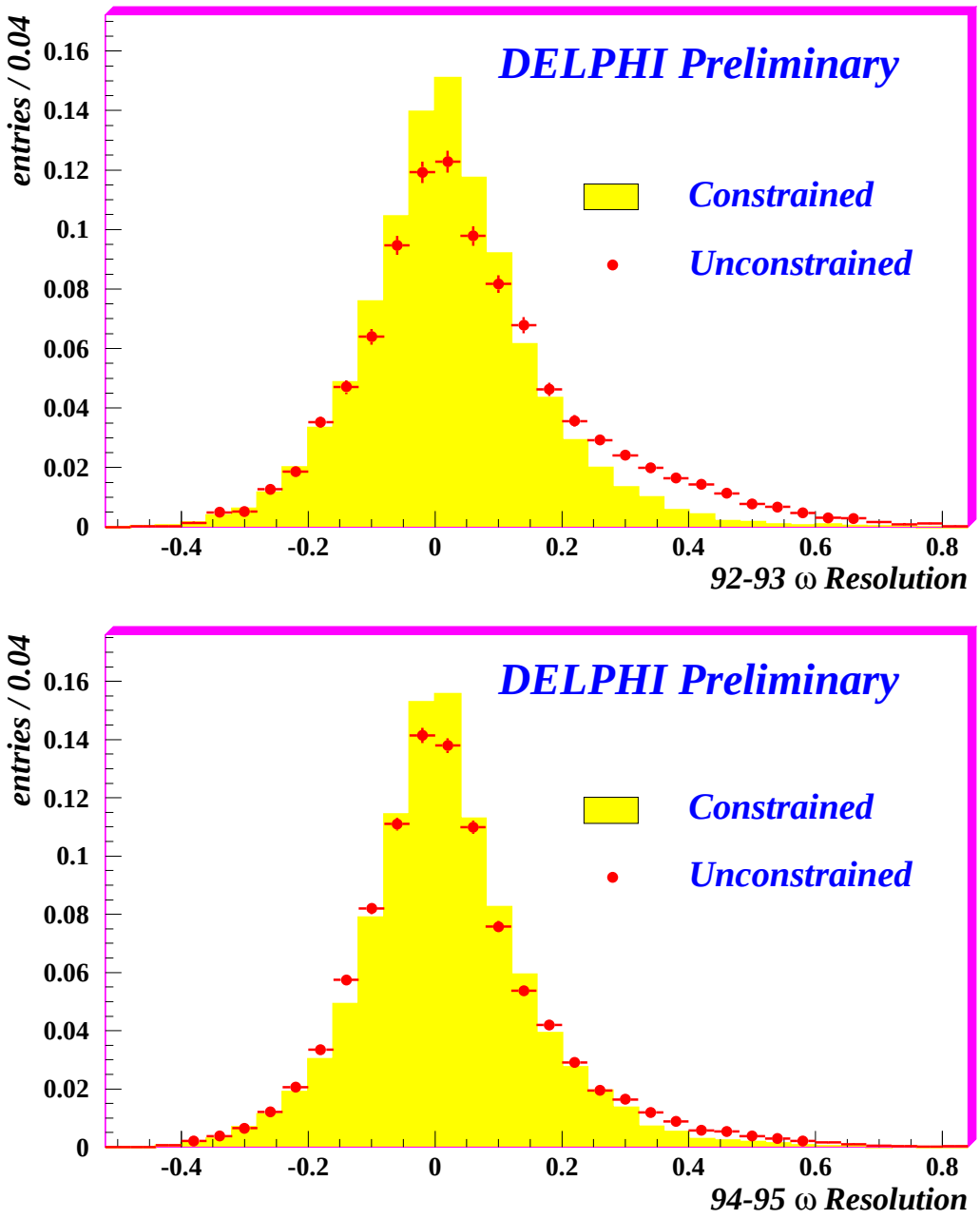

Figure 2: w resolution. Upper plot : 1992-1993 analysis; lower plot: 1994-1995 analysis. Dots: experimental resolution without exploiting kinematic constraints. Since 1994 three-dimensional vertex reconstruction helped improving the resolution.
Shaded area: further improvement due to the request $\mu^2 = 0$ (see text)

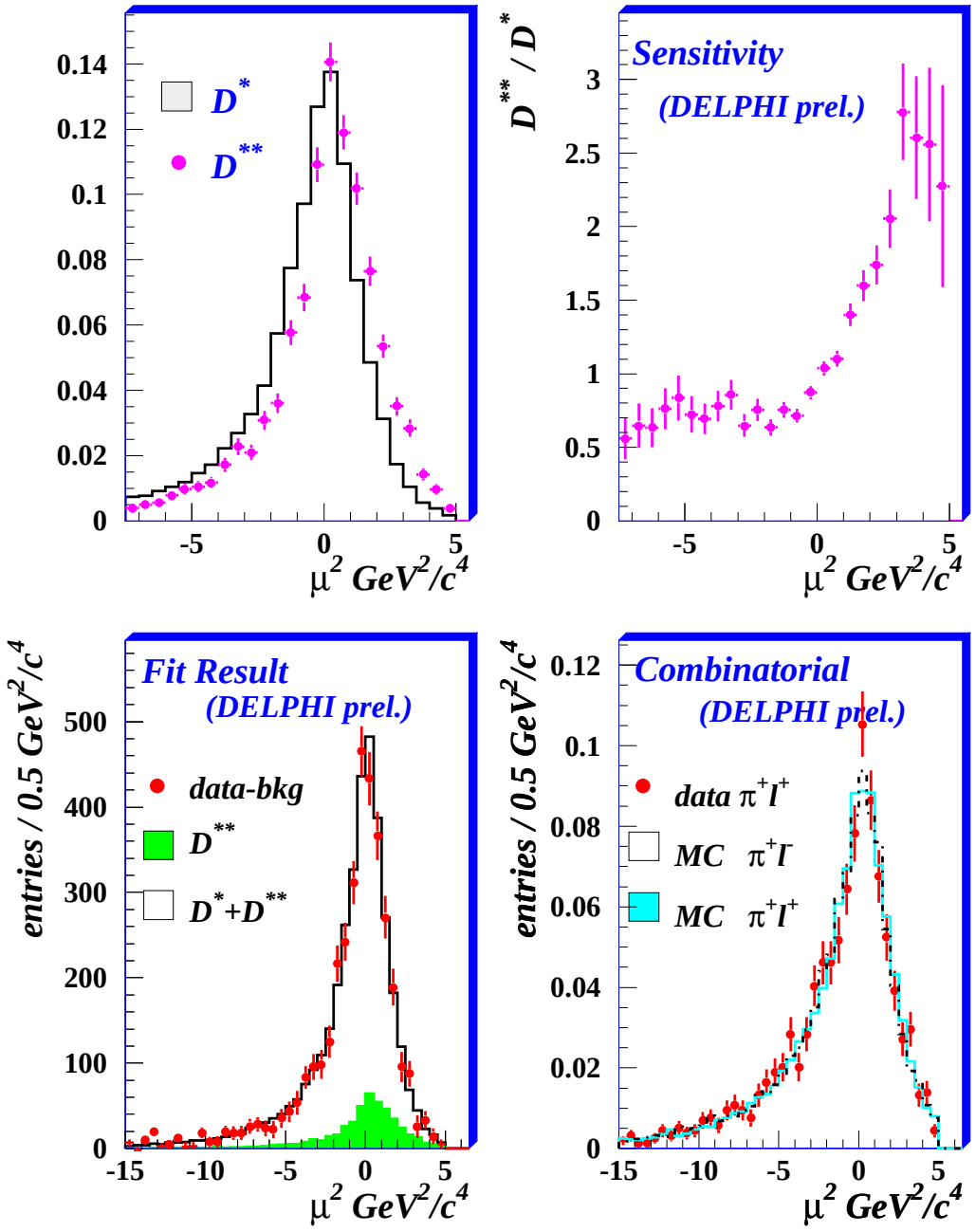

Figure 3: Determination of the D^{**} contamination.
Upper left: μ^2 distribution for D^{*+} (continuous line) and D^{**} events (arbitrary normalisation).
Upper right: ratio of the two distributions, showing the sensitivity of the method.
Lower left: fit results. Dots represent the data after subtraction of the background, the shaded area represents the fitted D^{**} contribution, the line contains the additional contribution by D^{*+} .
Lower right: combinatorial background for the wrong charge data (dots), the wrong charge simulation (solid line) and the good charge simulation (dotted line). A Kolmogorov test was applied to any couple of distributions providing $\sim 60\%$ agreement in all cases.

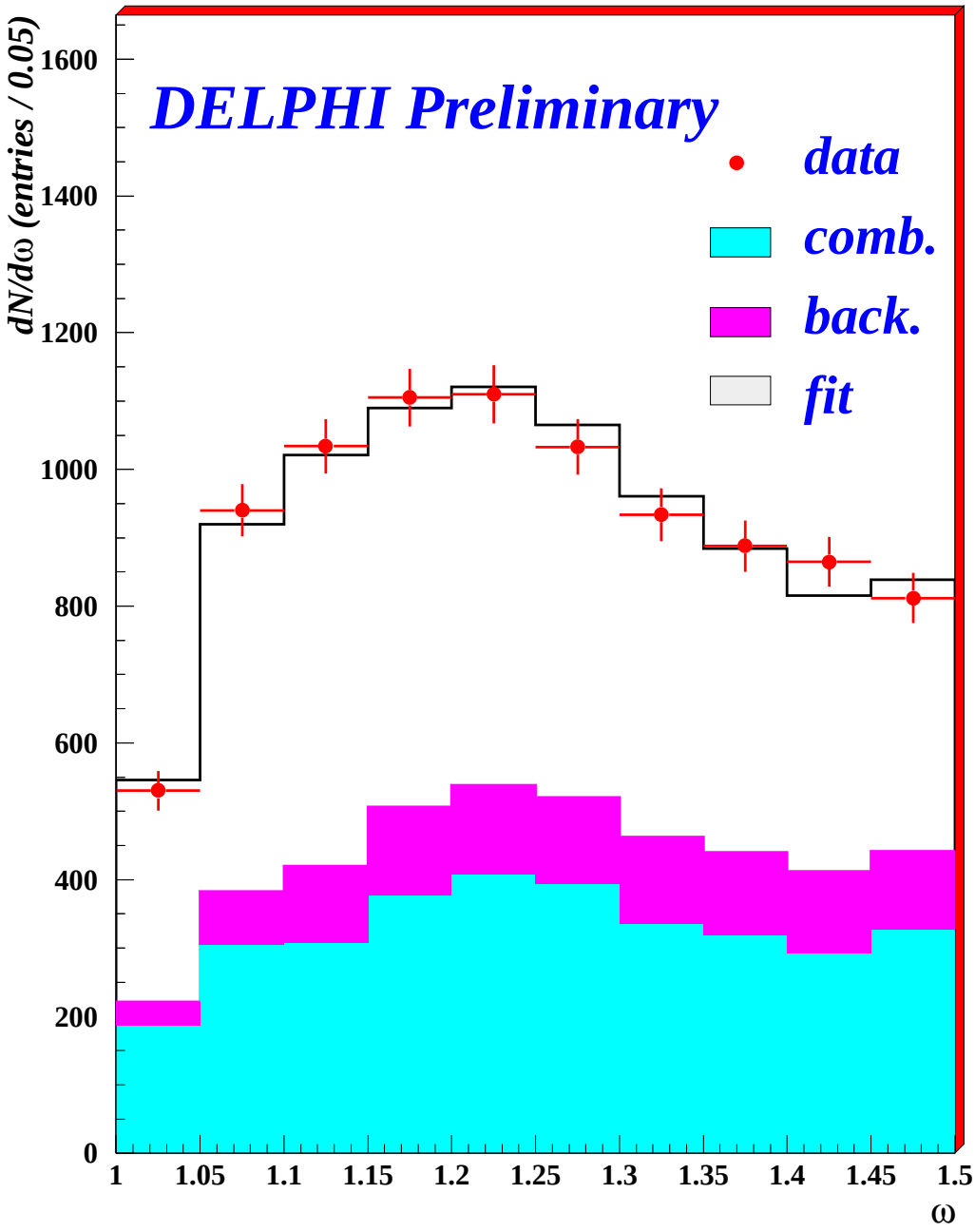

Figure 4: Fit to the w distributions. Dots with error bars: data; light shaded area: combinatorial background; dark shaded area: other backgrounds, including D^{**} ; histogram: all components, the unshaded area corresponds to the decay $\bar{B}^0_d \to D^{*+}\ell^-\nu$

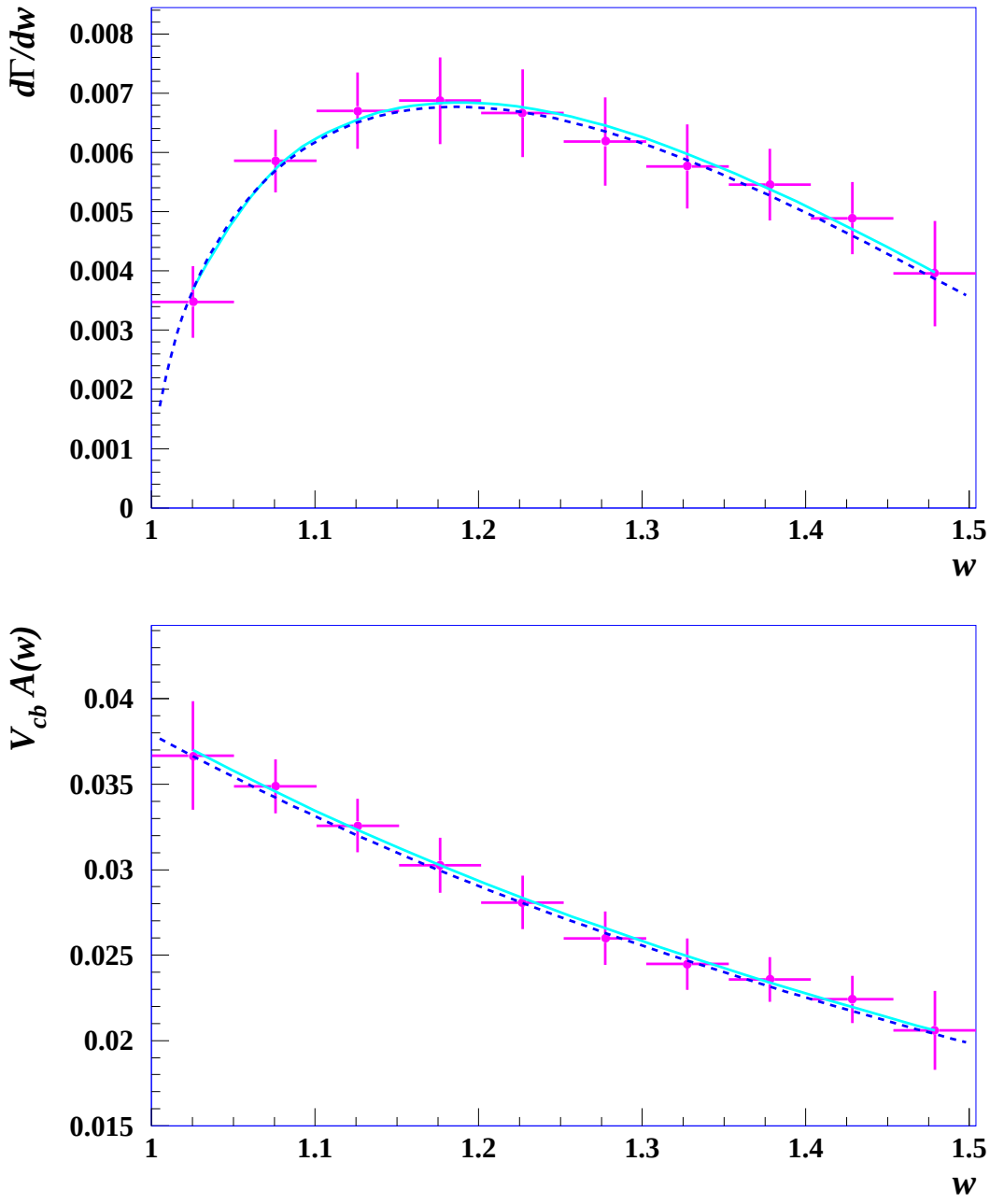

Figure 5: Unfolded distributions. Upper plot: differential decay width. Lower plot: decay form factor as in eq. (8). The continuous lines show the results of a fit to the histograms, neglecting bin to bin correlations. The dotted lines show the result obtained when including the statistical correlations among the bins.